Monthly Notices of the ROYAL ASTRONOMICAL SOCIETY

MNRAS **460,** 3706–3719 (2016) doi:10.1093/mnras/stw1106
Advance Access publication 2016 May 26

The conjectured S-type retrograde planet in ν Octantis: more evidence including four years of iodine-cell radial velocities

D. J. Ramm,[1]★ B. E. Nelson,[2] M. Endl,[3] J. B. Hearnshaw,[1] R. A. Wittenmyer,[4] F. Gunn,[1] C. Bergmann,[1] P. Kilmartin[1] and E. Brogt[5]

[1]*Department of Physics and Astronomy, University of Canterbury, Private Bag 4800, Christchurch 8140, New Zealand*
[2]*Center for Interdisciplinary Exploration and Research in Astrophysics (CIERA), Department of Physics and Astrophysics, Northwestern Institute for Complex Systems (NICO), Northwestern University, Evanston, IL 60208, USA*
[3]*McDonald Observatory, The University of Texas at Austin, Austin, TX 78712, USA*
[4]*Department of Astrophysics and Optics, School of Physics, University of New South Wales, Sydney 2052, Australia*
[5]*Academic Services Group, University of Canterbury, Private Bag 4800, Christchurch 8140, New Zealand*

Accepted 2016 May 6. Received 2016 May 6; in original form 2016 March 22

ABSTRACT

We report 1212 radial-velocity (RV) measurements obtained in the years 2009–2013 using an iodine cell for the spectroscopic binary ν Octantis (K1 III/IV). This system ($a_{\rm bin} \sim 2.6$ au, $P \sim 1050$ d) is conjectured to have a Jovian planet with a semimajor axis half that of the binary host. The extreme geometry only permits long-term stability if the planet is in a retrograde orbit. Whilst the reality of the planet ($P \sim 415$ d) remains uncertain, other scenarios (stellar variability or apsidal motion caused by a yet unobserved third star) continue to appear substantially less credible based on cross-correlation function bisectors, line-depth ratios and many other independent details. If this evidence is validated but the planet is disproved, the claims of other planets using RVs will be seriously challenged. We also describe a significant revision to the previously published RVs and the full set of 1437 RVs now encompasses nearly 13 yr. The sensitive orbital dynamics allow us to constrain the 3D architecture with a broad prior probability distribution on the mutual inclination, which with posterior samples obtained from an *N*-body Markov chain Monte Carlo is found to be $152.^{\circ}5 \pm^{0.7}_{0.6}$. None of these samples are dynamically stable beyond 10^6 yr. However, a grid search around the best-fitting solution finds a region that has many models stable for 10^7 yr, and includes one model within 1σ that is stable for at least 10^8 yr. The planet's exceptional nature demands robust independent verification and makes the theoretical understanding of its formation a worthy challenge.

Key words: techniques: radial velocities – planets and satellites: dynamical evolution and stability – binaries: spectroscopic – stars: individual: ν Octantis.

1 INTRODUCTION

It has been speculated from several years of radial-velocity (RV) observations that the single-lined spectroscopic binary (SB1) ν Octantis hosts a Jovian planet (Ramm 2004; Ramm et al. 2009). Given the present scale of exoplanet discoveries, this may not seem too unusual. However, the binary has by far the tightest geometry of any proposed to harbour a circumstellar (i.e. S-type) planet, having a mean separation of only $a_{\rm bin} \sim 2.6$ au. The minimum-separation barrier is presently tentatively at about 20 au, as will be described in more detail shortly. Furthermore, the RV signal, if it is caused by a planet, places its circumprimary orbit about mid-way between the stars i.e. $a_{\rm pl} \sim 0.5 a_{\rm bin}$. For a prograde orbit, models predict long-term stability should be limited to about half this distance i.e. $a_{\rm pl} \lesssim 0.25 a_{\rm bin}$ (Holman & Wiegert 1999; Ramm et al. 2009; Eberle & Cuntz 2010; Andrade-Ines et al. 2016). However, if the planet is in a retrograde orbit, as first suggested by Eberle & Cuntz (2010), the stability zone is wider (Jefferys 1974; Morais & Giuppone 2012), and places the conjectured orbit very near and perhaps within the boundary of stability. As extraordinary as the retrograde scenario may appear, since its very formation would also be challenged by strong dynamical interactions, the alternative standard explanations of instrumental or data reduction anomalies, star-spots, pulsations, or apsidal motion of the binary orbit are less supported by the observational evidence (Ramm et al. 2009; Ramm 2015). Other retrograde planets have been postulated but in each of these other cases a *choice* exists between viable prograde and

★E-mail: djr1817@gmail.com

Table 1. Stellar parameters for ν Oct. (1) Mermilliod (1991), (2) this work, (3) ESA (1997), (4) Costa et al. (2002), (5) Ramm et al. (2009), (6) Fuhrmann & Chini (2012). Fuhrmann & Chini (2012) revised the primary mass and radius estimates given in Ramm et al. (2009), based in particular on their metallicity. Their 2σ errors are halved here to be consistent with the 1σ errors used elsewhere here.

Parameter	ν Oct A	Reference
Spectral type	K0 III‡	(3)
V (mag)	3.743 ± 0.015	(1)
M_V (mag)	+2.02 ± 0.02	(2)
$(B-V)$	0.992 ± 0.004	(1)
H_p (*Hipparcos* mag)	3.8981 ± 0.0004	(3)
Mass ($\mathcal{M}_\odot$)	1.61	(6)
Radius ($\mathcal{R}_\odot$)	5.81 ± 0.12	(6)
$T_{\rm eff}$ (K)	4 860 ± 40	(6)
log g (cgs)	3.12 ± 0.10	(6)
[Fe/H](dex)	+0.18 ± 0.04	(6)
$v \sin i$ (km s^{-1})	2.0	(4),(6)
Age (Gyr)	∼2.5–3	(5)

‡We suspect the luminosity class may be evolved at most IIIb–IV (see the Discussion).

Table 2. Orbital parameters for ν Oct A and the conjectured planet from 222 RVs (Ramm et al. 2009) and *Hipparcos* astrometry. The Keplerian elements are the RV semi-amplitude K, period P, eccentricity e, and the argument of periastron ω. The scaled masses are based on the revised primary mass. Each relative orbit's semimajor axis a is derived from Kepler's third law, and assumes coplanar orbits.

	ν Oct A's absolute orbits	
companion	ν Oct B	Conjectured planet
K_1 (km s^{-1})	7.032 ± 0.003	0.052 ± 0.002
P (d)	1050.1 ± 0.1	417.4 ± 3.8
e	0.2359 ± 0.0003	0.12 ± 0.04
ω_1 (°)	75.05 ± 0.05	260 ± 21
i (°)	70.8 ± 0.9	–
Ω (°)	87 ± 1.2	–
$\mathcal{M} \sin i$	0.55 ($\mathcal{M}_\odot$)	2.4 ($\mathcal{M}_{\rm Jup}$)
a (au)	2.6 ± 0.1	1.3 ± 0.1
rms (m s^{-1})	19	
$(\chi^2_\nu)^{1/2}$	4.2	

retrograde options (see e.g. Gayon-Markt & Bois 2009; Goździewski et al. 2015), whilst no choice exists for ν Oct.

Nu Octantis (HD 205478 HIP 107089 HR 8254) has a slightly evolved early K-type primary with a late-dwarf or white-dwarf (WD) secondary (Table 1). The possibility of a planet was first mentioned in Ramm (2004) with 156 RVs and barely one binary orbit observed. The planet elements were approximated to $P \sim 400$ d, $e = 0$, $K \sim 60\,{\rm m\,s^{-1}}$, and $\mathcal{M}_{\rm pl} \sin i_{\rm pl} \sim 3\mathcal{M}_{\rm Jup}$. The tight orbital geometry and commonly found rotation period of evolved K-type stars led Ramm to surmise, though mostly on qualitative evidence, that rotational modulation of recent surface features was a more likely cause. With three more years of data, Ramm et al. (2009) identified the planetary hypothesis as having more support, this explanation though very precarious given the rapid instability of a prograde orbit. They claimed the then considered alternatives had less credibility because: (1) *Hipparcos* provided evidence of photometric stability ($H_p = 3.8981 \pm 0.0004$; ESA 1997), (2) there was no correlation of bisector values with the perturbation RVs, (3) the anticipated upper bounds of the rotation period and the need for unusually long-lived surface features, and (4) there was no evidence of significant activity, chromospheric or otherwise (Warner 1969; Slee et al. 1989; Beasley, Stewart & Carter 1992; Hünsch et al. 1996). Morais & Correia (2012) suggested the planet may be an illusion created by the system being instead a hierarchical triple, with ν Oct B being a binary and causing apsidal motion of the observed primary's orbit. This alternative, however, has no support from the already published orbits spanning 100 yr (Ramm 2004; Ramm et al. 2009).

The first orbital solutions for the conjectured system (Ramm et al. 2009) are summarized in Table 2. Combined with astrometry from *Hipparcos* (ESA 1997), the longitude of the line of nodes $\Omega_{\rm bin}$ and the inclination $i_{\rm bin}$ were also derived, the latter being one of the most precise estimates derived using this method. This preliminary solution, based on the understandable uncertainty of the underlying cause, was determined assuming only a simple double-Keplerian model.

The retrograde-orbit scenario for ν Oct has been explored in increasing complexity by Quarles, Cuntz & Musielak (2012) and Goździewski et al. (2013). Both studies conclude that stable retrograde orbits exist that obey the rather noisy observational constraints. As well as being the first to re-analyse the RVs with a self-consistent Newtonian model, Goździewski et al. (2013) also emphasized the complex chaotic space of narrow intersecting stability zones and relatively small islands of long-term stability. Furthermore, their stable models had to be significantly shifted from the N-body and Keplerian best-fitting models, implying the conjectured planet was inconsistent with the then available data.

Planets may exist in binary systems in either P-type (in the present context, circumbinary) or S-type (circumstellar) configurations. Of the confirmed binaries harbouring S-type planets, all have stellar separations exceeding that of ν Oct by an order of magnitude or so. Zhou et al. (2012) and Wang et al. (2014) identify the apparent barrier of about 20 au to such orbits based on the accepted planet-hosting binaries. These include GJ 86 A (Queloz et al. 2000), HD 41004 A (Zucker et al. 2004), and HD 196885 A (Correia et al. 2008; Thébault 2011). One of the first exoplanet claims were for γ Cephei A (Campbell, Walker & Yang 1988), which was then understandably challenged (Walker et al. 1992). 11 yr elapsed before Hatzes et al. (2003) provided evidence that vindicated that planet's reality. An S-type planet was claimed for α Cen B (Dumusque et al. 2012; $a_{\rm bin} \sim 17.5$ au) though the planet orbit is tiny ($a_{\rm pl} = 0.04$ au). Its existence has been challenged (Hatzes 2013) and more recently by Rajpaul, Aigrain & Roberts (2016). The planet claimed for the hierarchical triple HD 188753 (Konacki 2005; $a_{\rm bin} \sim 13$ au) also appears to be non-existent (Eggenberger et al. 2007). All accepted S-type systems have separation ratios much smaller than that implied for ν Oct, with γ Cep, HD 196885 and HD 41004 all having $a_{\rm pl}/a_{\rm bin} \sim 0.1$. It is thus hardly surprising that the ν Oct planet remains unconfirmed and controversial,[1] even though it may so far 'pass' many standard tests for such a claim, as the above-mentioned discredited planets also originally did.

Thus, there is no direct observational precedent for a planet to exist in such circumstances though, for instance Trilling et al. (2007) give some indirect evidence based on infrared excesses of main-sequence binaries. The ν Oct system also presents formidable theoretical challenges and many papers explore the formation and stability of S-type systems, such as Chauvin et al. (2011), Thébault

[1] Approximately 10 per cent (∼200) of present planet claims are in this category. See The Extrasolar Planets Encyclopaedia at http://exoplanet.eu.

(2011), Müller & Kley (2012), Jang-Condell (2015), and Rafikov & Silsbee (2015). The planet forming coevally with the present binary orbit is inconsistent with our present understanding of such processes, even if the original orbit was prograde. Rafikov (2013) studied planetesimal formation in small-separation binaries (again at the 'barrier' $a_{\rm bin} \sim 20$ au) and found that sufficiently massive axisymmetric discs may eliminate the fragmentation barrier for the formation of giant planets in these 'tight' systems. Whether or not these findings or related ones can ultimately extend to the extreme demands of ν Oct remains to be determined. Hence, it is not surprising that such tight binaries are rarely included in S-type planet search programmes, and this bias may underlie (though extremely unexpectedly) their lack of discovery.

Since coeval formation is presently so unbelievable, more credible alternatives must be considered, no matter how exotic they may presently seem. A strong gravitational event (e.g. a passing star) is not so exotic. This multifaceted possibility includes variations such as capture of one other star or a planet-hosting star. Dynamical captures or exchanges have been discussed by Pfahl & Muterspaugh (2006), and in the context of open cluster interactions by Portegies Zwart & McMillan (2005). Another variation is that the planet was originally hosted by the secondary and somehow exchanged (see e.g. Kratter & Perets 2012; not surprisingly, their work focused on more manageable binary models having e.g. separations of 75–105 au). Tutukov & Fedorova (2012) describe other atypical planet formation scenarios, including ones involving white dwarf companions in binaries and retrograde orbits created by passage of the host through a dense rotating molecular cloud.

This paper continues the search for the cause of the RV behaviour of ν Oct. In Section 2, we describe the nearly 13 yr of data and the two instrument setups, the second including a larger detector and iodine cell. Section 3 presents our RV data sets, including the new iodine-cell velocities acquired between 2009 and 2013, and a critical revision of the older cross-correlation function (CCF) RVs (2001–2007) reported in Ramm et al. (2009). We also provide preliminary orbital solutions, at this point abbreviations of our simple double-Keplerian model. In Section 4, we assess Ca II H lines, CCF bisectors, and line-depth ratios (LDRs). Section 5 provides our 3D dynamical orbital solutions, and our stability modelling results are given in Section 6. Section 7 discusses three additional system details: our derived space velocities, the benefits of future astrometry and imaging opportunities, and the nature of the system's initial discovery. The Discussion evaluates the various possible causes of the mysterious RV signal. The paper concludes that the hypothesis, that the RV signal is caused by a retrograde planet, still has the most support from the data.

2 OBSERVATIONS AND REDUCTIONS

2.1 Spectrograph and CCD detectors

All spectroscopic observations were obtained at University of Canterbury Mt John Observatory, Lake Tekapo, New Zealand using the 1-m McLellan telescope and the échelle spectrograph HERCULES (Hearnshaw et al. 2002; Ramm 2004). From the start of operations in 2001 until 2006/7 the detector was a 1k × 1k detector. Initial testing of a complete-wavelength-coverage 4k × 4k detector began in 2006 October. This detector was then removed briefly and the original detector used until the 4k × 4k CCD was installed permanently in early 2007.

2.2 Observations

As well as ν Oct's many favourable spectral and photometric characteristics for precise RVs, its airmass at Mt John Observatory (latitude 43° S) never exceeds 1.9 due to its far southern declination (∼−77°).

2.2.1 1k × 1k *CCD (2001 2007)*

In addition to the 222 observations (2001–2006) reported in Ramm et al. (2009), a further 21 spectra were obtained over four consecutive nights 2007 February–March between the detector changes described above and extend the time-span of observations with this detector to nearly 2100 d. It has also been decided to reject 18 of the Ramm et al. (2009) paper's spectra from our final analyses as it has been recognized that they were probably acquired in circumstances making their reliability and quality questionable.[2] Thus, 225 RV spectra were included from this detector, 215 with a resolving power $R \sim 70\,000$ and 10 with $R \sim 41\,000$. The typical exposure time for stellar spectra was 3–5 min which provided an average signal-to-noise ratio S/N = 122 ± 16 in the middle of order n = 110 ($\lambda \sim 5170$ Å).

2.2.2 4k × 4k *CCD (2006 2013)*

During the brief initial commissioning of this detector in late 2006 (but without the I_2 cell), two ν Oct spectra were taken on the night of October 15 (JD 245 4024). When this larger CCD was installed permanently in early 2007, the I_2 cell was included, positioned just before the Cassegrain focus. The cell was maintained at 50° C and provided a dense imprint of molecular absorption lines from 5000 to 6200 Å. This cell was replaced in 2011 March by one promising to provide somewhat stronger spectral lines.[3] A pinhole relay system was installed in 2011 March in front of the fibre entrance. The pinhole was included for the benefit of a parallel programme observing α Cen (Bergmann 2015; Endl et al. 2015), whose increasingly narrow angular separation contributed significant cross-contamination. The pinhole reduced the light throughput by about half and eventually (2013 April) it could be removed when required.

All spectra obtained with this detector used $R \sim 70\,000$. Stellar exposure times were generally 12–20 min with the pinhole, and 7–15 min without it. A total of 1180 spectra had iodine-cell RVs derived from them, having an average S/N = 113 ± 26. A further 32 spectra could only have a CCF RV derived, and fell into two groups: 22 RV exposures with S/N = 157 ± 44 and 10 Ca II -related exposures averaged 349 ± 49. Thus, there are 1233 new RV spectra reported from both detectors.

Initially only spectral orders n = 86–116 were recorded. From 2010 December, the readout was extended to n = 129, beyond which inadequate S/N was found for our standard RV exposures. These bluer orders promise more precise CCF RVs, and critically, would be needed for our CCF bisector measurements. These orders would also allow us to recover RVs for 4k × 4k spectra for which I_2-cell processing proved unachievable, and allow us to significantly improve the precision of the 1k × 1k RVs presented in Ramm et al. (2009, Sections 3.1.1 and 3.2).

[2] See Ramm (2015, Section 2.1.1) for an explanation of these additions and rejections.

[3] However, as Table 3 will reveal, the mean internal RV error for our ν Oct spectra actually increased by 0.7 m s^{-1} with this change.

Table 3. An abbreviated list of the 1180 AUSTRAL-processed I_2 spectra acquired during 2009–2013 using the 4k × 4k CCD including barycentric-corrected Julian date, corrected relative velocity V_{I_2}, internal error σ_i and barycentric correction, and the S/N in order $n = 110$. The entire table is provided online.

JD 245...	V_{I_2} (km s^{-1})	σ_i (m s^{-1})	bary.corr. (km s^{-1})	S/N ($n = 110$)
4854.1147	3.925	3.6	3.5271	84
4854.1190	3.926	3.6	3.5302	88
4854.1226	3.923	3.5	3.5329	89
4854.1270	3.931	3.7	3.5360	85
4855.1861	3.958	4.3	3.8538	72

2.3 Preliminary spectral reductions

The non-iodine part of each reduction was carried out using the Hercules Reduction Software Package (HRSP) v.3 for the 1k × 1k spectra (Skuljan 2004; also see Ramm 2004 for improvements to CCF RVs) and HRSP v.5 for the 4k × 4k spectra. Standard methods of échelle spectral reduction were utilized that included background subtraction and cosmic ray filtering. A quartz white lamp was used for flat-fielding and normalization. Th–Ar spectra were obtained immediately before and after the stellar exposures for wavelength calibration. This latter requirement was critical for the CCF-derived RVs, but substantially less important for the iodine-cell RVs, as the I_2 lines provide the wavelength calibration. An interpolated dispersion solution from the thorium spectra was calculated corresponding to the flux-weighted-mean observation time, t_{fwm}, the latter provided by an exposure metre. The t_{fwm} allowed HRSP to calculate the Julian-Day and RV barycentric corrections, which are the dates and RVs used throughout this paper.

3 RADIAL VELOCITIES

The 257 CCF and 1180 I_2 RVs give a total of 1437 RVs sampling a time-span of nearly 4600 d or about 12.5 yr. The method for deriving the 4k × 4k RVs is given first as it is conventional and straightforward. These I_2 RVs were also required for determining, by a novel strategy, the 257 CCF RVs with higher precision than had been previously achievable with HERCULES.

3.1 4k × 4k detector RVs

Three high-S/N iodine-free template spectra of ν Oct were co-added to form a single reference spectrum. Analysed in conjunction with high-S/N spectra of the relatively line-free B-stars β Centauri and α Eridani, all obtained close in time, this reference was deconvolved from the instrument profile using the maximum entropy method. The RVs were derived with the pipeline AUSTRAL (Endl, Kürster & Els 2000) using 14 orders. An abbreviated list of the final velocities, V_{I_2}, is given in Table 3. The mean error is 3.6 ± 0.5 m s^{-1}. We also include our barycentric corrections and S/N estimates for order $n = 110$.

3.1.1 Using I_2 RVs as a gauge to derive CCF RVs

32 4k × 4k spectra could not be fully processed by AUSTRAL. Instead, using the orders blueward of the I_2 forest, their RVs were derived using CCFs. Here, we describe the unconventional strategy used to derive the CCF-order weights to yield RVs with accuracies comparable to the I_2 RVs.

Table 4. An abbreviated list of the relative velocity data of 32 4k × 4k detector observations acquired 2006–2013 using CCF fitting. Columns as for Table 3. The table is reproduced in full online.

JD 245...	V_{CCF} (km s^{-1})	σ_i (m s^{-1})	bary.corr. (km s^{-1})	S/N ($n = 110$)
4024.1070	9.562	52	− 15.9816	123
4024.1202	9.557	52	− 15.9813	127
5728.2797	− 0.638	15	6.7807	186
5816.9981	1.626	12	− 13.7272	224
5819.9725	1.704	16	− 14.1085	117

Our only assumption was that the I_2 RVs are a far more accurate gauge than typical HERCULES CCF RVs, easily justified by the vast literature supporting this detail, and avoids the assumption of a specific model as Ramm et al. (2009) did. A continuous series of 561 4k × 4k stellar spectra was selected that provided I_2 RVs and the 16 non-I_2 orders $n = 114$–129. These covered a time-span approximating one binary period of ∼1050 d and thus the full range of ν Oct RVs. This series began on the first night the required bluer orders were recorded (JD 245 5534) and ended on JD 245 6566. They are identified in Fig. 3. A high-S/N spectrum was used as the reference to create the CCFs for these 16 orders n. We used the wider $n\lambda$ limits available with this larger detector (∼50 Å) and a Gaussian for fitting. The difference between the I_2 RV and the CCF RV for each order was calculated for the 561 spectra i:

$$\Delta V_{i,n} = V_{I_2,i} - V_{CCF,i,n},$$

and the corresponding standard deviation of these differences ($\sigma_{\Delta V}$) calculated, each difference weighted by the error on V_{I_2}. Our goal was to find the Gaussian that provided the smallest average of the 16 $\sigma_{\Delta V}$ values. This set of Gaussians increased in radius from the CCF core in steps of ±1 bin from a minimum $r_{gs} = \pm 4$ bins, to one that assured us the optimum radius had been identified.[4] The standard deviations for each order for the optimum radius determined its relative weight: $w_n = 1/\langle\sigma_{\Delta V}\rangle^2$. Finally, due to their differing reference spectra, the I_2 and CCF RVs have different velocity zero-points. Their offset, incorporated into the final published velocities, V_i, is $V_{off16} = -3.987 \pm 0.010$ km s^{-1}. The total error assigned to each CCF V_i was this offset error (±10 m s^{-1}) added in quadrature to the spectrum's internal error. The 32 4k × 4k CCF RVs are presented in Table 4. The mean error, not including the rather isolated first pair in 2006 October (JD 245 4024), is 16 ± 3 m s^{-1}. The substantially larger errors on the two RVs from 2006 are presumably related to their more distant acquisition time and the changing of the CCDs during 2006/7.

It is relatively simple to check if these CCF RVs are likely to be reliable, since we can assess their accuracy relative to I_2 RVs (Fig. 1). Whilst understandably of lower precision, these 19 CCF RVs have similar relative accuracy as their neighbouring I_2 RVs. Whilst these results are limited to a single star and this small sample, they suggest that if the weighting of the CCF orders is determined accurately, the resulting RVs can be of comparable accuracy to ones derived

[4] Our reduction software HRSP also allowed the use of third-order spline interpolation and parabolas of varying radii for CCF fitting. None of these provided as optimum a final result as that achieved with any Gaussian. The possibility of determining the best Gaussian radius separately for each order was not pursued for two reasons: (1) it would have added an extra layer of complexity to this analysis, and (2) the results we will soon describe provided CCF RV precision that seemed difficult to claim could be improved.

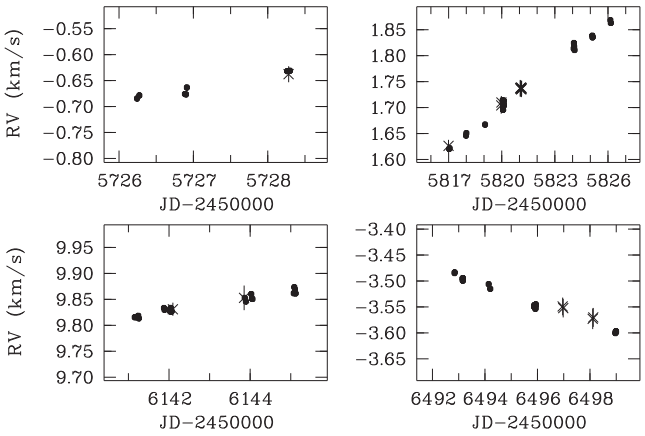

Figure 1. 19 CCF RVs (×) compared to all their neighbouring I_2 RVs (•) for the 4k × 4k detector. The vertical axis has a constant span of 300 m s^{-1} and any visible vertical lines are the corresponding 1σ limits.

with an I_2 cell. Assessing the credibility of the controversial ν Oct planet and any competing scenarios depends on RVs of the highest quality. Hence we will now apply this order-weighting strategy to the older 1k × 1k spectra reported in Ramm et al. (2009).

3.2 Revision of 1k × 1k CCF RVs

Unfortunately, the CCF RVs reported in Ramm et al. (2009) have several suspicious features that suggest a revision of them is prudent. For instance, the old internal errors (typically 4–6 m s^{-1}) are similar to our I_2-RV errors, a Keplerian model was used to derive the spectral order weights, and perhaps most suspicious of all, $(\chi^2_\nu)^{1/2} = 4.2$ (Table 2), easily accounted for by the likelihood the errors are underestimated.

To derive the CCF RVs from the 561 4k × 4k spectra, we now have to restrict the number of examined orders ($n = 114$–124) and the width of each order (∼20 Å) to match the older 1k × 1k spectra. Since the gauge and star are the same, and the only instrumental difference is the pixel size, which is identical across all orders for each detector, we claim the weighting strategy remains valid. The simple Keplerian solutions that duplicate the orbital fitting used in Ramm et al. (2009) will support this claim by nearly halving the solution rms.

A different reference spectrum to that used in Ramm et al. (2009) was used here, having a higher S/N ∼ 260, which promised somewhat better RV precision. To avoid the reference spectrum's internal error being zero (a consequence of the autocorrelation CCF process), all 1k × 1k spectra had a minimal jitter term of 3 m s^{-1} added in quadrature to their errors, this being approximately the average error for the I_2 RVs. This adjustment will be given careful reappraisal during the Markov Chain Monte Carlo (MCMC) dynamical orbit-fitting analysis to give a properly refined estimate of any jitter terms.

The internal errors have a number of characteristics that suggest significant improvements to the original ones (Fig. 2): (1) almost all are significantly greater than our I_2-RV errors [by a mean factor of about 3 ×, similar to the 2009 paper's suspicious $(\chi^2_\nu)^{1/2}$], (2) their mean magnitude (15 ± 4 m s^{-1}) is more consistent with the anticipated possible precision of a HERCULES-CCF orbital solution, and (3) their values cover a much wider range, a sensible reflection of the varied observatory conditions experienced by DJR during 2001–2006. An abbreviated list of these 225 revised CCF RVs is

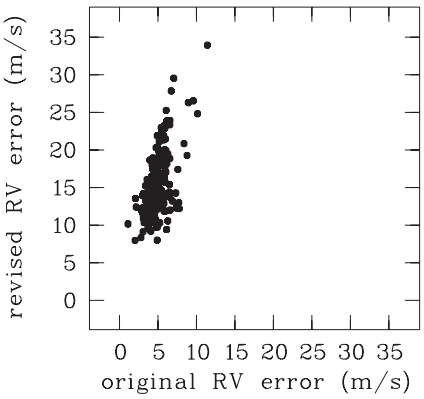

Figure 2. A comparison of the CCF RV errors for the 204 1k × 1k detector spectra common to this work and Ramm et al. (2009).

Table 5. An abbreviated list of the 225 spectra acquired during 2001–2007 using the 1k × 1k CCD. Columns as for Table 3. The entire table is provided online.

JD 245...	V_{CCF} (km s^{-1})	σ_i (m s^{-1})	bary.corr. (km s^{-1})	S/N ($n = 110$)
2068.0607	−0.346	34	8.6469	128
2102.1137	−2.047	19	0.0825	129
2121.0920	−3.256	13	−4.8861	137
2180.8839	−7.347	27	−15.3966	134
2219.8985	−9.581	18	−14.5397	96

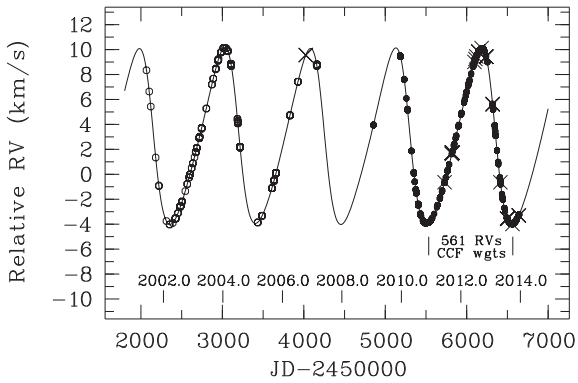

Figure 3. The complete set of 1437 ν Oct velocities 2001–2013: CCF RVs from the 1k × 1k detector '○'; I_2 RVs from the 4k × 4k detector '•', CCF RVs from the 4k × 4k detector '×' CCF RVs. The RVs are offset to a common zero-point for clarity of the illustration. The small overlap of RVs from the two detectors is evident near JD 4100. The series of 561 RVs used to re-evaluate the 1k × 1k RVs is identified (see Section 3.2).

provided in Table 5. A plot of all our 1437 velocities is given in Fig. 3.

3.3 Preliminary orbital solutions – Keplerian

Keplerian orbital solutions are not adequate to model the conjectured ν Oct system. However, they serve a useful purpose if some of their details are given immediately, for instance, to demonstrate the improved precision of the older CCF RVs (the goal of Section 3.2), and to illustrate the strong persistent RV signal that all competing scenarios must explain. The actual elements are not critical for the paper's progress except to point out they are in close agreement with the values reported by Ramm et al. (2009), in particular the

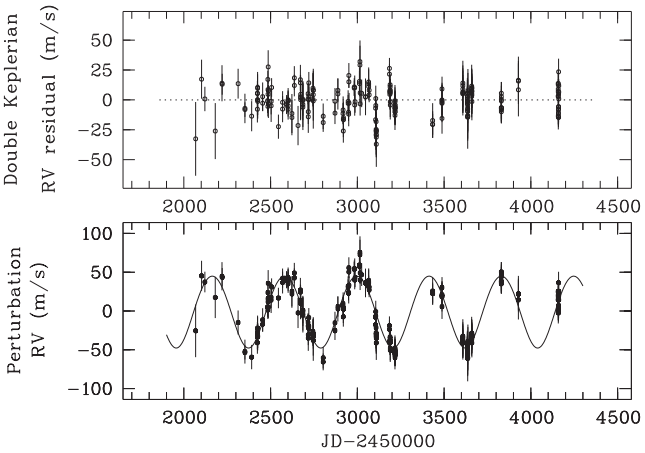

Figure 4. The conjectured planet's RVs determined using a double-Keplerian model including the RV residuals, for 225 1k × 1k detector spectra (2001–2007). The error bars represent 1σ limits.

elements of the conjectured planet include $P_{\rm pl} \sim 415$ d, $e_{\rm pl} \sim 0.03$, and $K_{\rm pl} \sim 45\,{\rm m\,s^{-1}}$. A Newtonian analysis of our RVs more appropriate to the conjectured strongly interacting system will be presented in Section 5. The Keplerian solutions were again derived using a time of zero-mean longitude T_0 as the reference epoch (Sterne 1941), where the mean longitude $L = \omega + M$, and M is the mean anomaly.

3.3.1 1k × 1k *detector*

Our re-evaluation provides a significant improvement to the precision of the 222 spectra reported in Ramm et al. (2009, see Table 2): the rms lowers to 14.4 m s^{-1} and $(\chi^2_\nu)^{1/2} = 1.02$. For the revised set of 225 RVs (having rejected the 18 suspect observations described in Section 2.2.1), the rms lowers further to 10.6 m s^{-1} (even though the data set's time-span is extended by 233 d by the additional 21 spectra obtained in 2007). These results give further justification for the rejected spectra even though they were never tested for outlier status. A plot of the corresponding RV curve and residuals is given in Fig. 4. This is the lowest orbital rms derived for CCF RVs obtained with HERCULES, which previously was limited to about 15 m s^{-1} for sharp-lined spectra (see e.g. Skuljan, Ramm & Hearnshaw 2004; Ramm 2008), and for the first time approaches the spectrograph's design specification for CCF RVs (10 m s^{-1}; Hearnshaw et al. 2002).

3.3.2 4k × 4k *detector*

A plot of the conjectured planet's RVs, the solution's best-fitting curve and the velocity residuals are given in Fig. 5. Besides confirming the existence of the originally reported ∼415 d RV signal, the residuals of the 32 I_2-calibrated CCF RVs have relative accuracies that are uniformly similar to those solely derived from the iodine lines and AUSTRAL. Furthermore, the earliest two RVs, near JD 245 4024, have large errors and make no significant contribution to the orbital solution. Their high relative accuracy to the final fit with and without them is further vindication for the method used to derive these CCF RVs. The RVs and errors allowed a solution with an rms of 6.5 m s^{-1} and $(\chi^2_\nu)^{1/2} = 1.83$. If a further jitter of 5 m s^{-1} is added in quadrature to the internal errors of all 1212 RVs the total jitter is about 6 m s^{-1}, a suitable value proposed by Johnson et al. (2010) for stars similar to ν Oct, and $(\chi^2_\nu)^{1/2} = 1.06$ is derived.

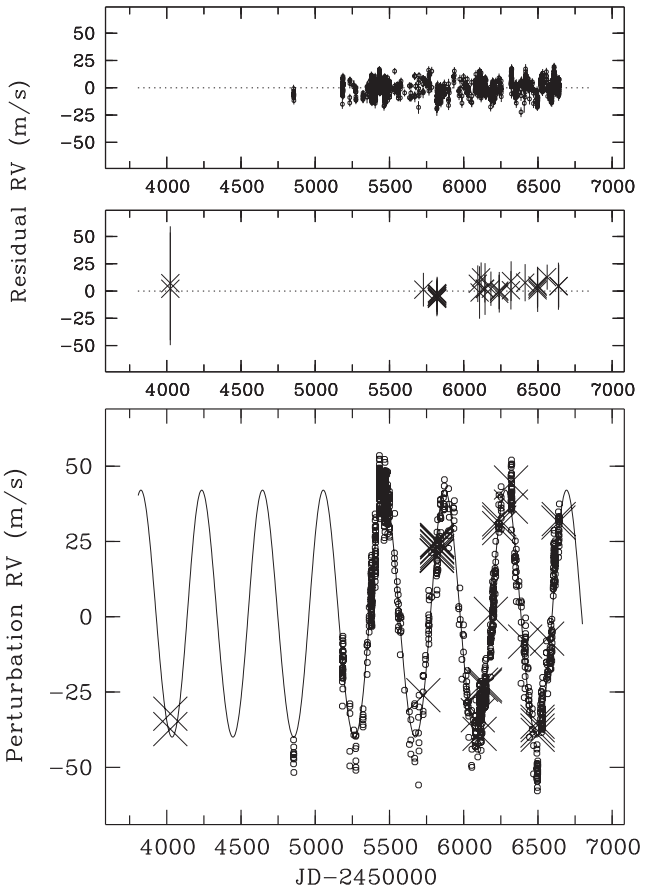

Figure 5. The conjectured planet's double-Keplerian-model RVs including RV residuals, 1212 4k × 4k detector spectra (2006–2013). The 1180 I_2-cell RVs are identified with '○'. The 32 CCF RVs are labelled with '×'. The error bars represent 1σ limits.

4 NON-RV SPECTRAL ANALYSES

Before describing the results of our dynamical orbital analyses, we next present our evidence re-affirming that this periodic RV signal is unlikely to have a stellar origin. The investigations include those for chromospheric activity using the Ca II H line, LDRs and CCF bisectors, sampling, respectively, short, long, and medium wavelengths.

4.1 Ca II H&K SPECTRA

The vast majority of the spectra taken with both CCDs either did not include the Ca II H&K orders, or did so with very inadequate S/N. Only one Ca II spectrum was acquired with the 1k × 1k detector owing to the need to manually move the detector to record these lines – time consuming and not ideal for obtaining precise RVs. Negligible chromospheric activity has been reported by Warner (1969) for spectra obtained during 1964–1965, whose eye-estimate value was '1' (the scale was 0–8 with 0 indicating absence of K-line emission).

With the 4k × 4k CCD, RV exposures were far too short to provide adequate S/N for the Ca II lines. Therefore, 17 longer exposures were taken at irregular intervals approximately consistent with the conjectured planet's RV cycle to monitor potential variability. Whilst our sample is relatively small, neither the H nor the K line shows any significant variability or any periodicity consistent with

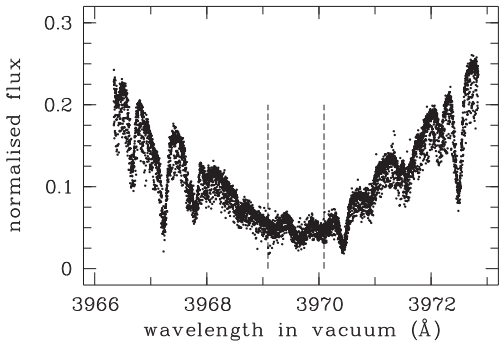

Figure 6. The central region of the Ca II H line for 17 HERCULES spectra recorded by the 4k × 4k detector from 2011 September 12 to 2013 December 18. The 1 Å window for measuring the total flux is identified.

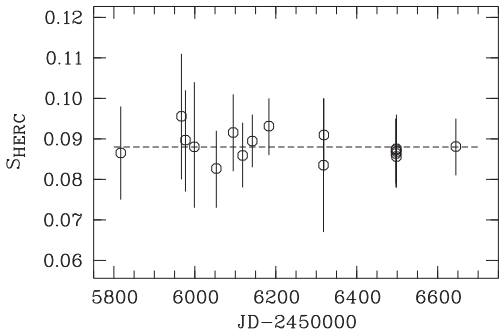

Figure 7. The Ca II H line ratios S_{HERC} of the 17 HERCULES spectra illustrated in Fig. 6. The vertical line through each ratio represents $\pm 1\varepsilon$.

the RV behaviour. The K line was less well exposed and so we restrict our attention to the H line.

We followed the general method of Santos et al. (2000). We measured the total flux of a 1 Å wide window centred on the Ca II H line ($\lambda_{vac} = 3969.59$ Å) and divided this by the total flux in a second region 15 Å wide centred at 3990 Å. An overlay of the 17 spectra in the vicinity of the Ca II H line is given in Fig. 6, after Doppler shifting has been taken into account.[5] The S/N estimated at the centre of the order including the H line varied considerably, having an average $\langle S/N \rangle = 96 \pm 25$. There was no correlation between S/N and the chromospheric-activity index S_{HERC}. The error ε for each ratio was estimated at 10 per cent[6] for S/N = 100, and then scaled accordingly: hence $\varepsilon_{(S_{HERC})} = 10 \times S_{HERC}/(S/N)$. The distribution of H-line ratios is given in Fig. 7. A Lomb–Scargle periodogram analysis was conducted and no periodicities significantly exceeding the background noise were found at any frequency, in particular at the RV-perturbation period ∼415 d, nor at the estimated rotation period of ν Oct A, $P_{rot} \simeq 140 \pm 35$ d (based on its radius, $v \sin i$ and making the simple but perhaps inaccurate assumption $i_{rot} = i_{bin}$).

4.2 Line-depth ratios

LDRs have a long but infrequent history for supporting or discrediting exoplanet discoveries e.g. 51 Peg (see e.g. Gray 1997; Hatzes, Cochran & Bakker 1998). In a recent paper, Ramm (2015) likewise investigated the 215 ν Oct spectra reported in Ramm et al. (2009), deriving 22 LDRs from 10 spectral lines in the wavelength region 6230–6260 Å. Spectra of 20 similarly evolved stars were also used to create a temperature scale. Ramm recovered the original 21 stellar temperatures with an accuracy and standard deviation of 45 ± 25 K and found no significant periodic behaviour in any of the LDRs.

Carefully constructed ratios are known to be extremely sensitive to temperature (see e.g. Gray & Johanson 1991; Gray & Brown 2001; Kovtyukh et al. 2003). Besides having no periodic behaviour, the 215 LDR-calibrated temperatures T_{ratio} had a standard deviation of only 4.2 K over the several years 2001–2007. Making the realistic assumption ν Oct A was therefore not likely to be pulsating, the temperatures were converted to magnitude differences Δm using the Stefan–Boltzmann law. The distribution of these have a striking similarity to the scatter recorded in the *Hipparcos* photometry obtained about 15 yr previously. We now extend this LDR analysis to the newer spectra.

Unfortunately, all of the LDR spectral lines utilized in Ramm (2015) occur in order $n = 91$, which, for the vast majority of our 4k × 4k spectra are swamped with iodine lines. However, 47 spectra were acquired without the iodine cell (some accidentally, some intentionally) on 21 nights during 12 observing runs spanning 2538 d (2006 October–2013 September), a useful additional sample. In order $n = 91$, 39 spectra have a mean S/N = 246 ± 62 and for the remaining eight it is 525 ± 46, the latter being part of the set of longer exposures for acquiring our Ca II spectra. Once again, from a Lomb–Scargle analysis, there is no periodic behaviour in this latest sample in the vicinity of the ∼415 d RV signal, none consistently across all of the 22 ratios, and none with power significantly greater than any periodogram's background noise.

Converting each ratio into a temperature using calibration stars allows the temperature to be derived more precisely by the averaging of all the results for each spectrum. These in turn can be converted to magnitude differences that can further act as a guide for assessing the reliability of the method. The average temperature for all 22 ratios is 4811 ± 28 K. This is consistent with the effective temperature reported by Fuhrmann & Chini (2012; 4860 ± 40 K). The 47 averaged temperatures have a mean of $T_{\nu\,Oct} = 4811 \pm 4.1$ K, practically identical to the value reported in Ramm (2015; 4811 ± 4.2 K).

Magnitude differences were derived and these again have a striking resemblance to the brightness variations recorded by *Hipparcos* and estimated by Ramm (2015), the three sets of Δm values now spanning about 23 yr (Fig. 8). It should be noted that our estimates for Δm are extremely sensitive to the temperature ratio $T_{ratio}/T_{\nu\,Oct}$: varying T_{ratio} by only 1 deg changes Δm by about 1 mmag. Such similar behaviour of three high-precision sets of Δm values would seem to be unlikely to be due to misguided analytical methods. It would also be surprising if, whilst much larger variations did exist, they only occurred in the years not sampled.

4.3 CCF bisectors

Spectral line bisectors (see e.g. Gray 1983; Hatzes et al. 1998; Povich et al. 2001; Gray 2005) and that of CCFs (Queloz et al. 2001; Dall et al. 2006; Baştürk et al. 2011) are both well-recognized means to assess if a star's surface dynamics and irregular features can significantly influence RVs, or to identify spectral contamination from previously unrecognized stellar companions (Wright et al. 2013). Bisectors have also been shown to vary in systematic ways with surface gravity (i.e. luminosity) and effective temperature (Gray

[5] These plots mimic the single spectrum reported in Ramm et al. (2009) for JD 245 3831 (2006 April).

[6] Santos et al. (2000) were using $R = 50\,000$ spectra and made this choice for one of their stars that had only one observation.

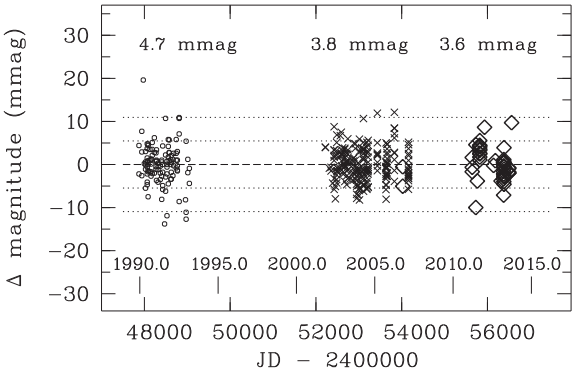

Figure 8. The magnitude differences, Δm, for ν Oct A based on 22 LDR calibrated temperatures: 215 1k × 1k spectra: '×', and 47 4k × 4k spectra: '◇'. All spectra acquired with resolving power $R = 70\,000$. These are compared to 116 best-quality *Hipparcos* observations (flag = 0: '○'). The dotted lines identify the $\pm 1.5\sigma$ and $\pm 3\sigma$ limits from the 1k × 1k predictions. The value above each data set is the Δm standard deviation.

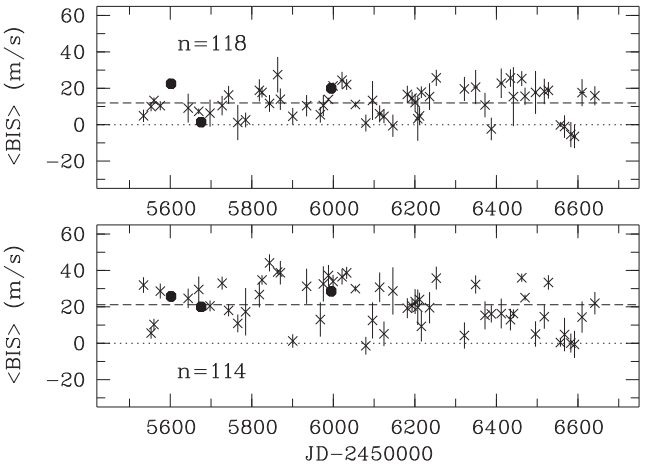

Figure 9. The mean BIS ($\langle$BIS$\rangle$) for 59 'observing runs' as defined in the text, derived from the CCFs of 675 spectra. Orders $n = 114$ and $n = 118$ are shown, together with their 1σ standard deviations. 'Observing runs' with only one BIS value are labelled with '•'. The average of each order's mean is represented by a dashed line.

2005; Gray 2010; Baştürk et al. 2011) though without the extreme sensitivity that for instance LDRs have for temperature.

Our bisectors were derived from 675 4k × 4k spectra (acquired 2010 December–2013 December) for the I_2-free orders with higher S/N, $n = 114$–120. The CCFs were created using a template spectrum with S/N ∼ 240. Five CCF flux levels were measured, at 20, 30, 45, 60, and 75 per cent of the CCF's parabola-fitted peak value. We constructed two variations of commonly used bisectors, the velocity span, $V_{\rm sp} = v_{30}$–v_{75}, and the bisector inverse slope BIS = $(v_{20} + v_{30})/2 - (v_{60} + v_{75})/2$. We found no evidence of any significant periodic behaviour for any order corresponding to the RV signal at ∼415 d from our Lomb–Scargle analyses, just as was reported in the previous CCF bisector analysis of Ramm et al. (2009). There is no correlation between the bisector values and the spectra's S/N.

To illustrate our bisector results, we concentrate on the BIS results. To provide them in a manner we believe is more revealing, we divided the spectra into sets defined to be separate 'observing runs'. Each 'run' only included spectra with no more than 3.5 d between consecutive dates. Typical observing runs lasted about a week and were separated by 2–4 weeks, but occasionally circumstances interrupted longer runs by several days (e.g. as a result of instrument failures or adverse weather), effectively separating groups of spectra. In most cases, the subsets of spectra represent true separate observing runs. About half of these subsets included eight or more spectra, and the maximum number of nights included in a single 'observing run' was 14 (two runs).

We derived the mean BIS $\langle$BIS$\rangle$ and standard deviation for the 59 allocated 'observing runs'. We reproduce the results for $n = 114$ and $n = 118$ as these have the least variability (Fig. 9). The standard deviation of the mean values $\sigma_{\langle \rm BIS \rangle}$, for many subsets is very low, and averages $5 \pm 3\,{\rm m\,s^{-1}}$, or about 5 per cent of the total BIS range for that order.[7] For both orders, only two spectra were rejected (their BIS values were treated as outliers as they each were about 4σ from the mean). For the 10 runs that included 20 or more spectra (to a maximum of 67 spectra), $\sigma_{\langle \rm BIS \rangle} \sim 7 \pm 2\,{\rm m\,s^{-1}}$, and for the two runs that extended over 14 nights $\sigma_{\langle \rm BIS \rangle} \sim 8\,{\rm m\,s^{-1}}$. The $\langle$BIS$\rangle$ values for these two orders have ranges significantly less than the RV signal's amplitude and are only weakly correlated ($r = 0.36$), whereas the 675 RVs are perfectly correlated ($r = 1.000$). Thus, we claim, critically, that most of the scatter for each order is not due to measurement errors, otherwise the scatter would presumably be evident in the individual runs. Since our spectra can easily reveal the signal in our CCF RVs ($K_{\rm pl} \sim 40$–$45\,{\rm m\,s^{-1}}$), we also claim that these very small 'observing run' standard deviations imply that we should be able to easily detect the perturbation signal in our CCF bisectors if it was present. The distribution of BIS mean values seems more likely to be due to acquisition variations, a result of the reduction process and/or stellar variability unrelated to the RV signal.

[7] This low fraction, a few percent, was found for all seven orders.

5 DYNAMICAL ORBITAL SOLUTIONS

We derived dynamical orbital solutions for the 225 1k × 1k detector RVs and the full set of 1437 RVs, the latter being the global solution we desire for our stability modelling. We characterize the masses and orbits of the ν Oct components using an N-body differential evolution MCMC (RUN DMC; Nelson, Ford & Payne 2014a), which incorporates the Swarm-NG framework to integrate planetary systems on Graphics Processing Units (Dindar et al. 2013). We adopt our prior probability distribution and likelihood function from Nelson et al. (2014a). Additional orbital parameters now include the primary star's mass $\mathcal{M}_1$, each companion's mass ($\mathcal{M}_2$ and the conjectured planet $\mathcal{M}_{\rm pl}$), and the mean anomaly M at our chosen epoch, plus the RV zero-point offset δV, and jitter $\sigma_{\rm jit}$, all based in a Jacobi coordinate system. The binary-orbital solution reported in Ramm et al. (2009) provides a precise estimate of the binary's longitude of line-of-nodes $\Omega_{\rm bin}$ and its inclination $i_{\rm bin}$ (Table 2) and therefore our reported orbital models fixed these two parameters. We also performed a similar run for each case that did not impose astrometric constraints and found the parameter estimates to be quantitatively similar. RUN DMC has been used to analyse other strongly interacting planetary systems while allowing for mutual inclinations (e.g. 55 Cancri, Nelson et al. 2014b; Gliese 876, Nelson et al. 2016). On one hand, ν Oct has a much lower dimensional model (i.e. only three bodies and fewer offset/jitter parameters); on the other hand, the proximity of these masses suggests the presence of extremely strong gravitational interactions, which can result in a posterior distribution that is very difficult to sample from.

Table 6. Dynamical solutions for ν Oct A and its conjectured planet using 225 CCF RVs from 1k × 1k detector observations (2001–2007). Estimates are computed using 15.9, 50, and 84.1 percentiles. Φ_{Bb} is the mutual inclination and χ^2_{eff} is the standard χ^2 with an additional penalty based on the jitter value similar to that described in Nelson et al. (2014a).

	ν Oct A's absolute orbit	
Companion	ν Oct B	Conjectured planet
$\mathcal{M}(\mathcal{M}_\odot)$	$0.584\,8 \pm 0.0003$	$0.002\,5 \pm 0.0003$
K_1 (km s^{-1})	$7.0514 \pm {}^{0.0047}_{0.0056}$	$0.0465 \pm {}^{0.0063}_{0.0041}$
e	$0.236\,48 \pm {}^{0.000\,61}_{0.000\,70}$	$0.116 \pm {}^{0.078}_{0.067}$
ω_1 (°)	$75.01 \pm {}^{0.15}_{0.16}$	$94 \pm {}^{55}_{227}$
P (d)	$1050.92 \pm {}^{0.46}_{2.18}$	$418 \pm {}^{19}_{17}$
a (au)†	$2.630\,00 \pm {}^{0.000\,70}_{0.003\,61}$	$1.283 \pm {}^{0.038}_{0.036}$
Ω (°)	87.0 (fixed)	$252 \pm {}^{38}_{15}$
i (°)	70.8 (fixed)	$100 \pm {}^{19}_{46}$
M (°)	$339.26 \pm {}^{0.15}_{0.14}$	$183 \pm {}^{227}_{50}$
Φ_{Bb} (°)	$147 \pm {}^{11}_{27}$	
rms (m s^{-1})	11	
χ^2	$152.2 \pm {}^{6.1}_{5.7}$	
χ^2_{eff}	$138.4 \pm {}^{6.1}_{5.6}$	
RV offset (m s^{-1})	$-6044.0 \pm {}^{1.8}_{0.6}$	
jitter (m s^{-1})	$0.81 \pm {}^{1.2}_{0.6}$	

†The semimajor axis is of the relative orbit $a = a_A + a_{comp}$.

Considering the lessons from Nelson et al. (2014a) regarding how to explore parameter space efficiently, we set the following algorithmic parameters for RUN DMC: $n_{chains} = 300$, $\sigma_\gamma = 0.01$, and MassScaleFactor = 1.0. We set our integration time-step to roughly 84 min and use the time-symmetrized Hermite integrator (Kokubo, Yoshinaga & Makino 1998). The epoch of these solutions is the time of the first observation, i.e. JD 245 2068.0607 for each data set.

We sampled from the Markov chains after they had burned-in sufficiently and obtained a set of posterior samples. For the RVs acquired only with the 1k × 1k detector, summary statistics of the model parameters are given in Table 6 and corresponds to $(\chi^2_\nu)^{1/2} = 0.85$. A similar table for the total set of RVs are given in Table 7 and has $(\chi^2_\nu)^{1/2} = 0.99$.

6 STABILITY MODELLING

Our posterior samples were integrated for 10^6 yr using a Jacobi-coordinate-system variant of the general Bulirsch–Stoer (B-S) integrator in the *N*-body dynamics package MERCURY (Chambers 1999). A B-S integrator, similarly used by Goździewski et al. (2013) in their detailed analysis of the ν Oct system, is appropriate given the assumed geometry includes a nearby massive secondary-star perturber, and which makes for instance the 'hybrid' integrator unsuitable. Nothing remained dynamically stable past our integration baseline.

6.1 Grid search for stable models: methods and results

Given the lack of promising results with our posterior samples, a grid search was also undertaken. The grid was created from the planet best-fitting planet elements a, e, i, ω, and M, encompassing $\pm 3\sigma$ across a uniformly divided range for each. Since Ω_{pl} was relatively precise compared to the other orbit angles, it was also kept constant. The grid was composed of $9 \times 15 \times 13 \times 11 \times 10 = 193\,050$ models, the respective grid steps were $\Delta a_{pl} = 0.004\,12$ au, $\Delta e_{pl} = 0.015$, $\Delta i_{pl} = 1°$, $\Delta\omega_{pl} = 10°$, and $\Delta M_{pl} = 10°$. The binary elements, which have relatively very high precision, were kept constant at their best-fitting values.

Table 7. Dynamical solutions for the ν Oct A and its conjectured planet using all 1437 HERCULES observations (2001–2013). See Table 6 for some explanations.

	ν Oct A's absolute orbit			
companion	ν Oct B		Conjectured planet	
$\mathcal{M}(\mathcal{M}_\odot)$	$0.585\,22 \pm 0.000\,04$		$0.002\,01 \pm 0.000\,02$	
K_1 (km s^{-1})	$7.055\,44 \pm {}^{0.000\,40}_{0.000\,44}$		$0.038\,74 \pm {}^{0.0009}_{0.0012}$	
e	$0.236\,80 \pm 0.000\,07$		$0.086 \pm {}^{0.043}_{0.036}$	
ω_1 (°)	74.970 ± 0.016		$350 \pm {}^{8}_{25}$	
P (d)	$1050.69 \pm {}^{0.05}_{0.07}$		$414.8 \pm {}^{3.6}_{2.6}$	
a (au)	$2.629\,59 \pm {}^{0.000\,09}_{0.000\,11}$		$1.276 \pm {}^{0.007}_{0.005}$	
Ω (°)	87.0 (fixed)		$237.8 \pm {}^{0.8}_{0.6}$	
i (°)	70.8 (fixed)		$112.5 \pm {}^{2.4}_{1.5}$	
M (°)	$339.286 \pm {}^{0.023}_{0.019}$		$301 \pm {}^{22}_{7}$	
Φ_{Bb} (°)	$152.5 \pm {}^{0.7}_{0.6}$			
rms (m s^{-1})	8.4			
χ^2	$1396.2 \pm {}^{53.7}_{54.4}$			
χ^2_{eff}	$2969.9 \pm {}^{7.9}_{5.5}$			
Detector	RV method	N	RV offset (m s^{-1})	jitter (m s^{-1})
1k × 1k	CCF	225	t $-6045.4 \pm {}^{1.1}_{1.0}$	$4.1 \pm {}^{2.4}_{2.9}$
4k × 4k	CCF	32	$2644.5 \pm {}^{2.7}_{2.9}$	$1.2 \pm {}^{2.1}_{0.8}$
4k × 4k	I_2	1180	$2642.01 \pm {}^{0.29}_{0.32}$	$5.89 \pm {}^{0.17}_{0.18}$

Given the models' exceptional geometry, the choice of a reliable time-step τ was also given careful consideration. Ultimately it was decided a suitable strategy was to process the entire grid for several time-steps. Small but, critically, insignificant survival-time differences for each model would give us confidence that the integrator was likely to be reliable for this extreme system. The shortest time-step was relatively brief, 0.4 d ($\sim 10^{-3} P_{pl}$), and the three others were simply prime numbers 3, 7, and 11 d, these chosen to be integers and non-integer multiples of any other. Finally, for the two boundary time-steps 0.4 and 11 d, we extended our integration times to 10^6 yr. The resulting survival times were indeed very similar.[8]

The time-step chosen for the grid results reported here, $\tau = 11$ d, was therefore not at all apparently critical, but being less CPU-time demanding, it was the only time-step that had its maximum integration time extended further, for all models to 10^7 yr. The model did not survive if the planet (1) travelled beyond 5 au (about twice a_{bin}; 89 per cent of the models), (2) collided with the central/primary star (5 per cent), or (3) collided with the secondary (0.3 per cent). Thus, about 5 per cent of our grid models (9786 models) survived to 10^7 yr. Most of the grid parameters (i.e. a_{pl}, e_{pl}, i_{pl}, M_{pl}) have gently sloping distributions across their entire ranges for the fraction of survivors to 10^7 yr. The mean longitude $L = \omega + M$ distribution differed in that it was strikingly symmetric and narrow. This symmetry gave us further confidence that our B-S integrator was reliable. The fraction of models surviving to 10^3, 10^5 and 10^7 yr are illustrated

[8] For instance, for the four time-steps, the mean number of survivors to 10^3 yr was $35\,351 \pm 24$ and to 10^5 yr it was $17\,334 \pm 52$. The survival times for the individual models were within 5 per cent of each other in nearly 85 per cent of them.

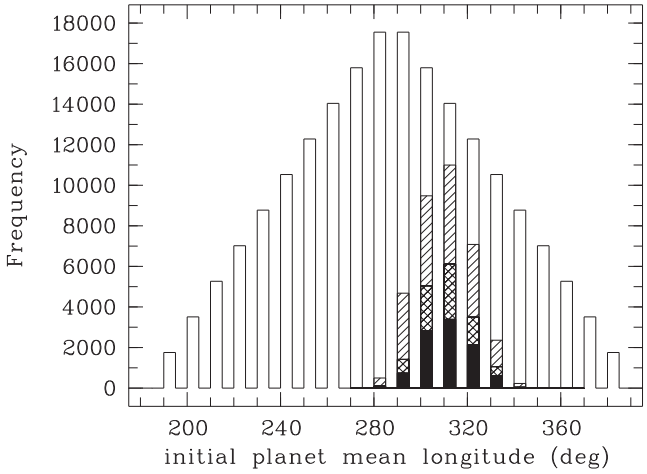

Figure 10. Histogram of the full grid of initial mean longitudes L for our 193 050 stability models with a time-step of 11 d. The lightly hatched subset survived to 10^3 yr (35 327 models), the double hatched to 10^5 yr (17 281 models), and the bold to 10^7 yr (9786 models). $L > 360°$ has been plotted to more easily illustrate the distributions.

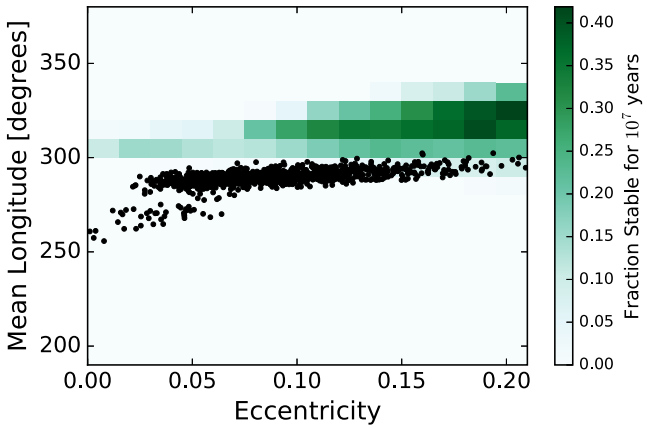

Figure 11. Grid search results in planet mean longitude and eccentricity space. Darker shades represent a higher fraction of stable systems residing within that particular cell (colour scale on right). Black dots are posterior samples. The online version is in colour.

in Fig. 10. The models most likely to survive, even to 10^3 yr, had initial $L_{\rm pl} = 310° \pm 10°$.

The distribution of stable models with respect to the planet's initial eccentricity and mean longitude is included in Fig. 11. We find higher eccentricities tend to provide more stable models. One model that survived to 10^7 yr had grid values all within 1σ of the best-fitting elements. Due to our computer-time limitations, only this one had the integration time extended to a little beyond 10^8 yr. One model survived the full integration for two time-steps, 0.4 and 11 d, but the planet was ejected at 35 and 91 Myr for the 3- and 7-d time-steps, respectively. This model's parameter set is given in Table 8.

7 OTHER CONSIDERATIONS

The controversial ∼415-d RV signal demands every possible characteristic of ν Oct be considered. Here, we discuss the system's space velocities, future imaging and astrometry, and the nature of the conjectured planet's discovery.

Table 8. The single model found to survive 10^8 yr within 1σ of our dynamical solution's best fit (given in Table 7). The component masses were $\mathcal{M}_1 = 1.61\ \mathcal{M}_\odot$, $\mathcal{M}_2 = 0.585\,22\ \mathcal{M}_\odot$, and $\mathcal{M}_{\rm pl} = 0.002\,01\ \mathcal{M}_\odot = 2.1\ \mathcal{M}_{\rm Jup}$.

companion	a (au)	e	i (°)	ω (°)	Ω (°)	M (°)
ν Oct B	2.629 59	0.2368	70.8	75.0	87.0	339.3
planet	1.272 61	0.12	115.0	355.0	237.8	315.0

7.1 Space velocities and age estimate

The conjectured ν Oct planet poses a challenge with regards its formation and some dynamical process such as a gravitational event including a passing star would appear to be amongst the most likely. Hence it seems worthwhile to determine ν Oct's present space velocities, although these results presumably place only a weak constraint on any past event. Quite reliable estimates should be achievable given the recent updating of all the required parameters. Space velocities inconsistent with the estimated age might imply such a dynamical process was more likely, though clearly too violent an event would completely disengage all the system's components.

The improved barycentric RV γ, parallax ϖ, and proper motions from Ramm et al. (2009) have been used to re-assess the heliocentric space velocities (U, V, W) and the corresponding probability of ν Oct's membership of the thin or thick disc as an age indicator.[9] The calculation was performed using the procedure described in Bensby, Feltzing & Lundström (2003) together with the equatorial coordinates (ESA 1997), yielding $U = +7.53 \pm 0.16\,{\rm km\,s^{-1}}$, $V = -41.43 \pm 0.26\,{\rm km\,s^{-1}}$, and $W = -11.62 \pm 0.11\,{\rm km\,s^{-1}}$. These velocities were then converted to the local standard of rest (LSR): $U_{\rm LSR} = +17.5\,{\rm km\,s^{-1}}$, $V_{\rm LSR} = -36.2\,{\rm km\,s^{-1}}$, and $W_{\rm LSR} = -4.5\,{\rm km\,s^{-1}}$ (see Dehnen & Binney 1998). These values in fact differ insignificantly from those reported by Bartkevičius & Gudas (2002). When plotted on a Toomre diagram, ν Oct is placed on the outer edge of the intermediate-age thin-disc population (age ∼ 3–4 Gyr), in close agreement with that given in Table 1.

7.2 Future astrometry and imaging

Any dynamical orbital solutions, stability studies, and efforts to understand the possible formation scenarios will also be able to be conducted with greater confidence if ν Oct's stellar masses and astrometry are more accurately determined. Ideally, this should be done in an as model-free manner as possible. Direct imaging and astrometric observations would also help to define the true nature of ν Oct B since the contrast observed would determine if it was a late-type main-sequence star or a WD. Assuming the stellar components are coeval, if ν Oct B is found to be a WD, which presumably could also reveal itself by a UV excess, it would have had to evolve much faster than the present primary, shedding at least one solar mass in the process (the mass difference of the present stellar components).

Since an astrometric orbit for the binary of reasonable quality has now been determined, in principle, the stellar masses can be derived by a single astrometric observation (the angular separation ρ and the position angle θ). One such interferometric observation was

[9] $\gamma = +35.24 \pm 0.02\ {\rm km\,s^{-1}}$; $\varpi = 45.25 \pm 0.25$ mas; $\mu_\alpha \cos\delta = +52.58 \pm 0.53$ mas/yr; $\mu_\delta = -240.80 \pm 0.47$ mas/yr: note the correction to the sign of μ_δ given in Ramm et al. (2009).

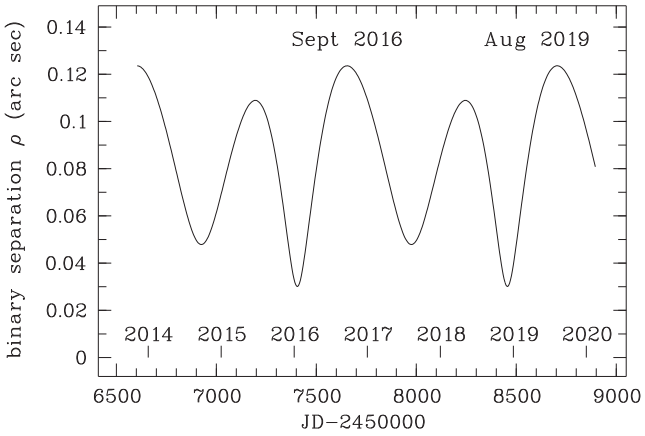

Figure 12. Predicted separations of the stellar components of ν Oct based on its parallax (Ramm et al. 2009) and our dynamical orbital elements given in Table 8.

reported several decades ago. Unfortunately, whilst Morgan, Beckmann & Scaddan (1980) claimed success with their single observation ($\rho = 0''.104$, $\theta = 331^\circ$), and their separation is approximately consistent with our prediction ($\rho \sim 0''.12$), their position angle is not, since we derive $\theta \sim 272^\circ$, thus making their claim questionable. The predicted angular separation has just passed a minimum and will achieve its next maximum in 2016 September (Fig. 12). Modern instruments should be able to make the necessary observations, particularly if ν Oct B is a higher contrast main-sequence star. Our derived mass for the secondary star, if it is unevolved, corresponds to a late K or early M dwarf having $M_V \sim 8$–9 mag, thus ν Oct B may be only 6 mag or so fainter than ν Oct A. A large series of astrometric observations would help better define the entire AB orbit, including for instance Ω_{bin} which we fixed for our dynamical analyses but may be more inaccurate than we suppose. Finally, such observations may also reveal any previously unknown stellar companions, such as the hierarchical triple scenario proposed by Morais & Correia (2012).

7.3 Serendipity

The HERCULES spectrograph is clearly capable of providing high-precision RVs and has been in service for 15 yr, yet the ν Oct planet is the only one so strongly proposed from its spectra. What are the chances such an extraordinary planet could be discovered in these circumstances? One would imagine they would be very slim indeed. So we ask, just as Wright et al. (2013) queried their discovery of the near face-on binary in MARVELS-1, how can we make the proposed discovery somewhat more plausible? In the first instance, given the Mt John telescope's relatively small aperture (1-m), any planet-hunting programme is seriously disadvantaged as compared to those using much larger apertures in more favourable observing sites. Consequently, such programmes have rarely been attempted at Mt John (but see Murdoch, Hearnshaw & Clark 1993). Instead many HERCULES-based projects study, for instance, pulsating stars and binaries with relatively short periods (often less than that of ν Oct). These are not ideal or typical targets for planet hunting. However, ν Oct is a suitable object for assessing HERCULES's long-term RV precision, being a very bright, sharp-spectral-lined SB1 (and previously having a low-precision orbital solution), is easily circumpolar at Mt John, and was known to be a very constant star. Hence it was included in the first HERCULES project (Ramm 2004). The ∼415 d RV signal was then easily found once it was adequately observed. The serendipitous discovery was aided by its far southern declination making ν Oct less easily observed at many other facilities (though it was initially included in the Pan-Pacific Planet Search; Wittenmyer et al. 2011). The remaining surprise may then be limited to the fact that something which is presently exceptional and so presumably quite rare, is so relatively nearby.

8 DISCUSSION

This work demonstrates that the extraordinary retrograde planet in ν Oct, whilst not yet definitively proven, remains the most credible of the known possible scenarios for the RV signal first described by Ramm (2004). Credibility for the planet now arises primarily from several independent high-precision observational methodologies.

The first evidence is the RV signal itself, now demonstrated to be persistent for nearly 13 yr (2001–2013), and using different strategies for deriving the RVs (CCFs and I_2 lines). The rms of our solution for all 1437 RVs is 8 m s^{-1} with $\chi^2 = 0.99$ (see Section 5). Similar but better long-term RV precision has been achieved with the single stars δ Pav and τ Cet during the parallel observing campaign mentioned in Section 2.2.2. For instance, the RVs from observations of τ Cet ($N = 1377$) acquired over nearly six years (2008–2014), have an rms of 4.6 m s^{-1}, and the median single-night rms ($N \geq 10$ per night) is 2.7 m s^{-1} (Bergmann 2015). Hence the signal cannot be due to instrument errors or the like – for instance it is also not present in RVs derived for the similar SB1 β Reticuli (K2 IIIb) studied in nearly identical circumstances from 2001–2007 (Ramm 2004; Ramm et al. 2009).

As well as our large new data set of high-precision I_2 RVs, the favourable revision of the previously published CCF RVs, is expected to have been helpful for our dynamical orbit and stability modelling and for future studies. The orbits derived are consistent with those reported by Ramm et al. (2009), at least with regards the observer-independent elements a, e, and P. These three elements are at the heart of the controversial claim for the ν Oct planet since they place its orbit, on average, mid-way between the stellar components having $a_{bin} \sim 2.6$ au.

8.1 Luminosity class of ν Oct A

The primary star of ν Oct is somewhat evolved from the main sequence but we wonder if it truly is a giant as is typically claimed i.e. K0 III (e.g. ESA 1997) or K1 III (e.g. Gray et al. 2006). Cool giants are known to have cyclic RV variability periods of the order of hundreds of days and RV amplitudes of 50–600 m s^{-1} (Walker et al. 1989; Cummings 1998; Hatzes & Cochran 1998). Cool subgiants, whilst less well understood in terms of surface dynamics (Hatzes et al. 2003), are generally less dynamically active than true giants, so the luminosity class of ν Oct A has some significance. The absolute magnitude of ν Oct A ($M_V = +2.02$) is maybe as much as two magnitudes fainter than MK-type normal giants of luminosity class III, the latter having their locus bounded more or less by $-1.5 \lesssim M_V \lesssim +0.5$. The absolute magnitude and spectral type suggest ν Oct A is instead no more evolved than luminosity class IIIb–IV (see fig. 1, Keenan & Barnbaum 1999). Also, as well as having many other characteristics similar to ν Oct A, the planet-hosting γ Cep A has M_V only 0.5 mag less, and is now classified K1 IV (Fuhrmann 2004). If a re-classification of ν Oct A is valid, just as was later realized for γ Cep A, our present understanding of such less evolved stars is

another reason why significant surface dynamics would seem less likely (Hatzes et al. 2003; Walker 2012).

8.2 Surface dynamics

Regardless of ν Oct A's true luminosity class, no evidence consistent with any kind of significant surface dynamics has been found over several decades and at multiple wavelengths e.g. in radio (Beasley et al. 1992), microwave (Slee et al. 1989), visible (*Hipparcos* 1992), and X-rays (Hünsch et al. 1996), and for Ca II emission (Warner 1969; Ramm et al. 2009). Pérez Martínez, Schröder & Cuntz (2011) identify ν Oct A as having an Mg $h+k$ chromospheric emission-line surface flux very close to their empirically derived basal flux of their sample of 177 cool giants. Our investigations of Ca II H-line emission, CCF bisectors and LDRs are also all consistent with the primary star having negligible dynamical surface behaviour. The LDR and bisector results challenge any possibility that surface-activity cycles or pulsations are the cause: both here and in Ramm (2015) the extremely temperature-sensitive LDRs converted to magnitude differences Δm strikingly mimic the *Hipparcos* photometric variations. Furthermore, the predicted spot-filling factor $f_{\rm sp} \sim 1$ per cent from the Δm values (see Ramm 2015, fig. 10) can be used to estimate the corresponding RV amplitude (see Hatzes 2002). Whilst the predictions of Hatzes were based on solar-type stars, since they were apparently applicable for the study of other non-solar-type stars e.g. HD 13189 (K2 II; Hatzes et al. 2005), we claim they are equally valid here. The predicted amplitude ($\sim$15 m s^{-1}) is about 3 × smaller than that observed.

Two other details related to the unlikely possibility of surface dynamics being involved. First, as Ramm et al. (2009) first noted, if the RV signal is related to star-spots, this would have to be both persistent – now extending to 12.5 yr – and geometrically fortuitous to be able to produce the near-sinusoidal RV signal. Secondly, the estimated period of rotation of ν Oct A $P_{\rm rot} \sim 140 \pm 35$ d, is about one-third of the RV signal's period. This estimate assumes $i_{\rm rot} = i_{\rm bin}$, which is presumably less likely to be true if a significant gravitational event has been involved in this system's history. Establishing a reliable and accurate rotational period $P_{\rm rot}$ for the star will help to decide if star-spots have any remaining credibility, though the obvious challenge will be achieving this for what seems to be an unspotted and only slightly evolved star. The same arguments seem to challenge the somewhat more mysterious macroturbulent regions proposed by Hatzes & Cochran (2000) for the RV behaviour of the faster rotating Cepheid-type variable Polaris and further discussed in relation to the planet-hosting massive K-giant HD 13189 (Hatzes et al. 2005). Pulsations are also challenged by the lack of any observational evidence (e.g. no cyclic photometric or LDR-temperature variations). Finally, our Newtonian solutions repeat the finding in Ramm et al. (2009) that the orbital period of the binary and conjectured planet may be close to a simple 5:2 ratio. This would be a somewhat unexpected coincidence if the eventual cause has a stellar origin.

8.3 Hierarchical triple-star scenario

Our orbital solutions also provide new evidence against the possibility that ν Oct is instead a hierarchical stellar triple. As mentioned in the Introduction, Morais & Correia (2012) presented this as an explanation, claiming the tell-tale evidence would be an apsidal precession rate $\Delta\omega_{\rm 1} = -0\overset{\circ}{.}86\,{\rm yr}^{-1}$. This is not supported by any orbital solutions. We have updated $\omega_{\rm 1}$ from our full dynamical analysis ($\omega_{\rm 1} = 75\overset{\circ}{.}0 \pm 0\overset{\circ}{.}2$; Table 7). We compared this to $\omega_{\rm 1}$ derived from a subset of the 21 historical RVs (Campbell & Moore 1928; Jones 1928). We selected the first 13 RVs which are confined to 1904–1911 (JD 241 6640–JD 241 9317), which provide a slightly more precise (and hopefully more accurate) $\omega_{\rm 1}$ than with all 21 RVs. We derived $\omega_{\rm 1} = 67\overset{\circ}{.}0 \pm 12^{\circ}$ for the zero-mean-longitude epoch JD 241 7272. A single-Keplerian orbit was derived since that is all these few low-precision RVs can justify. Between this epoch and that defined in Table 7, the time of the first modern RV ($\sim$JD 245 2068), is a time-span of 95 yr. The apsidal precession Morais & Correia (2012) predict over this time-span is about -82°, which clearly is not the calculated difference between these two $\omega_{\rm 1}$ values. The historical RVs have very low precision, but it seems they are easily capable of disclosing such a difference if it existed.

To further test the prediction by Morais & Correia (2012), we fitted a precessing Keplerian model to the full set of RVs. In this model, we fitted the secondary's orbit as a Keplerian orbit that is allowed to precess with time, with a precession rate of $\dot{\omega}$. This term is not governed by any particular physical mechanism such as general relativity, a stellar quadrupole, or tidal effects. It is merely a free parameter that we will constrain from the RV data.

Given the large signal to noise of the secondary star, we adopted uniform prior probability distributions in an arbitrarily large range for all of our model parameters (P, K, e, ω, M, $\dot{\omega}$, etc.). We performed an affine-invariant MCMC (Foreman-Mackey et al. 2013) to sample from the posterior distribution using a likelihood function similar to as described in Nelson et al. (2014a). After burning-in sufficiently, we sampled from the Markov chains and constrained $\dot{\omega} = +0\overset{\circ}{.}009\,51 \pm 0\overset{\circ}{.}000\,06\ {\rm yr}^{-1}$. Not only is this result two orders of magnitude off from the prediction, but it is also in the opposite direction (i.e. a prograde precession).

8.4 Stability modelling

Our stability studies have provided mixed results for credibility for the planet. On one hand, the observations provided very precise orbital and mass constraints for a retrograde planet model. However, none of the posterior samples were dynamically stable for 10^6 yr. One might suggest that we are actually witnessing a system on the brink of orbital destabilization, but given the time-scale of instability compared with the age of the star, this would be highly improbable. Several trial runs of the observations revealed many local minima which could easily trap our Markov chains depending on our set of initial conditions. It is possible, therefore, that our results are based on samples from a local rather than the true global minimum, which, based on the results of Goździewski et al. (2013), would not be too surprising.

The grid search revealed a region of parameter space with a higher probability of long-term stability. Whilst our grid identified only a relatively small fraction of models surviving to 10^7 yr ($\sim$5 per cent), and the majority of those somewhat distant from the best-fitting solution, one model whose grid values are all within 1σ of the best fit (Table 8) was stable to at least 35 Myr for our grid's four time-steps, and stable beyond 10^8 yr for two of them ($\tau = 0.4$ and 11 d). If the conjectured system's formation arose from a short-lived gravitational event (e.g. a passing star), the mutually inclined orbit, rather than a coplanar one, would seem to be more consistent with that possibility. A hypothesis of a moderate mutual inclination could also provide other significant advantages for more quickly resolving the true nature of the enigmatic ν Oct system e.g. in the form of verifiable predictions for orbit evolution of the binary and/or the conjectured planet such as Kozai-like mechanisms (Kozai 1962).

9 CONCLUSION

Definitive independent evidence is essential for deciding the fate of this controversial planet. Spectra acquired with much higher S/N and resolving power (and overall fidelity) will help to decide the credibility of any stellar-origin scenarios, and additional preferably more precise RVs will better define the conjectured orbit and facilitate better predictions of its evolution.[10] This can lead to a re-investigation of a self-consistent Newtonian model that also incorporates the *Hipparcos* and future astrometry. If the planet's existence is confirmed, a theoretical explanation will be needed. A gravitational interaction with a single or multiple bodies would presumably require the least, if any, revision to our present understanding of such scenarios. Some other migration process involving the stars or their planetary companion/s may also be applicable, though as with all formation scenarios, this too would seem to be a challenging one. If these options proved not to be viable, then ν Oct would instead aggressively confront our present understanding of coeval planet formation in such tight binaries, regardless of the system's original configuration. For many, the latter would be a very difficult scenario to believe. It is perhaps, however, prudent to recall that not so long ago (the 1980s and even early 1990s) it would have been almost as hard to believe hot-Jupiter exoplanets existed either, or indeed that there was any sense looking for exoplanets anywhere (Walker 2012).

Evidence against the planet should be as equally robust as evidence for it, since, if it is real but wrongly dismissed, we would presumably lose or at least delay our many opportunities for the future study of its exceptional characteristics. If the planet is non-existent, but all the astrometric, spectroscopic and photometric evidence is accurate, the consequences quite likely *exceed* that arising from the planet's reality. We would have to acknowledge that there is a new variation of stellar behaviour or orbit-related process that is consistent with all the current evidence. Such a discovery would have far-reaching consequences, both as a discovery in itself, but as a significant challenge to the existence of many other already *and* yet-to-be claimed RV-detected planets, perhaps regardless of the host star's evolution.

ACKNOWLEDGEMENTS

The Mt John programme was generously funded by Marsden Grant UOC 1007 administered by the Royal Society of New Zealand. The project was also supported in part by the Australian Research Council Discovery Grant DP110101007 (RW and FG). The authors thank McDonald Observatory, University of Texas at Austin for sharing the Sandiford iodine cell. The authors acknowledge the contribution of the New Zealand computer and analytics services NESI (New Zealand eScience Infrastructure), funded jointly by NeSI's collaborator institutions and through the Ministry of Business, Innovation, and Employment (URL http://www.nesi.org.nz). DJR thanks François Bissey for his support using these High-Performance Computing facilities at UC. We thank Stuart Barnes for his enthusiasm establishing the early work of this iodine-cell campaign and Jovan Skuljan for his efforts reconfiguring his reduction software HRSP for the larger 4k × 4k detector. BEN thanks Eric Ford, Jason Wright, and Trifon Trifonov for useful conversations about various interpretations of the data. DJR also thanks Gerald Handler for helpful discussions relating to pulsating stars, Trifon Trifonov for identifying a data anomaly and other useful comments, and Aleksandra Jarmolik for many helpful discussions including, on the lighter side, her recommendation to read Stanisław Lem's 'Solaris', curiously related to this work on several levels. We also appreciated the support of all staff at the Mt John Observatory. Our work has benefited from the data bases provided by SIMBAD, VizieR (CDS, France) and the NASA ADS.

[10] See e.g. Fischer et al. (2016) for the state-of-the-art of RV precision and its future goals and challenges. The work of Wright & Eastman (2014) identifies one avenue of review of our RVs based on the barycentric corrections, which we have no reason to suspect are significantly inaccurate, but which we have provided for this purpose.

REFERENCES

Andrade-Ines E., Beaugé C., Michtchenko T., Robutel P., 2016, Celest. Mech. Dyn. Astron., 124, 405
Bartkevičius A., Gudas A., 2002, Balt.Astron., 11, 153
Başturk Ö., Dall T. H., Collet R., Lo Curto G., Selam S. O., 2011, A&A, 535, 17
Beasley A. J., Stewart R. T., Carter B. D., 1992, MNRAS, 254, 1
Bensby T., Feltzing S., Lundström I., 2003, A&A, 410, 527
Bergmann C. M., 2015, PhD thesis, Univ. Canterbury
Campbell W. W., Moore J. H., 1928, Lick Obs. Publ., 16, 315
Campbell B., Walker G. A. H., Yang S., 1988, ApJ, 331, 902
Chambers J. E., 1999, MNRAS, 304, 793
Chauvin G., Beust H., Lagrange A.-M., Eggenberger A., 2011, A&A, 528, 8
Correia A. C. M. et al., 2008, A&A, 479, 271
Costa J. M., da Silva L., Nascimento J. D., Jr, de Medeiros J. R., 2002, A&A, 382, 1016
Cummings I. N., 1998, PhD thesis, Univ. Canterbury
Dall T. H., Santos N. C., Arentoft T., Bedding T. R., Kjeldsen H., 2006, A&A, 454, 341
Dehnen W., Binney J. J., 1998, MNRAS, 298, 387
Dindar S., Ford E. B., Juric M., Yeo Y. I., Gao J., Boley A. C., Nelson B. E., Peters J., 2013, New Astron., 23, 6
Dumusque X. et al., 2012, Nature, 491, 207
Eberle J., Cuntz M., 2010, ApJ, 721, L168
Eggenberger A., Udry S., Mazeh T., Segal Y., Mayor M., 2007, A&A, 466, 1179
Endl M., Kürster M., Els S., 2000, A&A, 362, 585
Endl M. et al., 2015, Int. J. Astrobiology, 14, 305
ESA 1997, ESA SP-1200: The Hipparcos and Tycho Catalogues. ESA, Noordwijk
Fischer D. et al., 2016, PASP, 128, 066001
Foreman-Mackey D., Hogg D. W., Lang D., Goodman J., 2013, PASP, 125, 306
Fuhrmann K., 2004, Astron. Nachr., 325, 3
Fuhrmann K., Chini R., 2012, ApJS, 203, 30
Gayon-Markt J., Bois E., 2009, MNRAS, 399, L137
Goździewski K., Słonina M., Migaszewski C., Rozenkiewicz A., 2013, MNRAS, 430, 533
Goździewski K. et al., 2015, MNRAS, 448, 1118
Gray D., 1983, PASP, 95, 252
Gray D. F., 1997, Nature, 385, 795
Gray D. F., 2005, PASP, 117, 711
Gray D. F., 2010, ApJ, 710, 1003
Gray D. F., Brown K., 2001, PASP, 113, 723
Gray D. F., Johanson H. L., 1991, PASP, 103, 439
Gray R. O., Corbally C. J., Garrison R. F., McFadden M. T., Bubar E. J., McGahee C. E., O'Donoghue A. A., Knox E. R., 2006, AJ, 132, 161
Hatzes A. P., 2002, Astron. Nachr., 323, 392
Hatzes A. P., 2013, ApJ, 770, 133
Hatzes A. P., Cochran W. D., 1998, ApJ, 502, 944
Hatzes A. P., Cochran W. D., 2000, AJ, 120, 979
Hatzes A. P., Cochran W. D., Bakker E. J., 1998, ApJ, 508, 380

Hatzes A. P., Cochran W. D., Endl M., McArthur B., Paulson D. B., Walker G. A. H., Campbell B., Yang S., 2003, ApJ, 599, 1383
Hatzes A. P., Guenther E. W., Endl M., Cochran W. D., Döllinger M. P., Bedalov A., 2005, A&A, 437, 743
Hearnshaw J. B., Barnes S. I., Kershaw G. M., Frost N., Graham G., Ritchie R., Nankivell G. R., 2002, Exp. Astron., 13, 59
Holman M. J., Wiegert P. A., 1999, AJ, 117, 621
Hünsch M., Schmitt J. H. M. M., Schröder K.-P, Reimers D., 1996, A&A, 310, 801
Jang-Condell H., 2015, ApJ, 799, 147
Jefferys W. H., 1974, AJ, 79, 710
Johnson J. A., Howard A. W., Bowler B. P., Henry G. W., Marcy G. W., Wright J. T., Fischer D. A., Isaacson H., 2010, PASP, 122, 701
Jones H. S., 1928, Cape Ann., 10, 237
Keenan P. C., Barnbaum C., 1999, ApJ, 518, 859
Kokubo E., Yoshinaga K., Makino J., 1998, MNRAS, 297, 1067
Konacki M., 2005, Nature, 436, 230
Kovtyukh V. V., Soubiran C., Belik S. I., Gorlova N. I., 2003, A&A, 411, 559
Kozai Y., 1962, AJ, 67, 591
Kratter K. M., Perets H. B., 2012, ApJ, 753, 91
Mermilliod J.-C., 1991, VizieR On-line Data Catalog: II/168. Institut d'Astronomie, Universite de Lausanne
Morais M. H. M., Correia A. C. M., 2012, MNRAS, 419, 3447
Morais M. H. M., Giuppone C. A., 2012, MNRAS, 424, 52
Morgan B. L., Beckmann G. K., Scaddan R. J., 1980, MNRAS, 192, 143
Müller T. W. A., Kley W., 2012, A&A, 539, 18
Murdoch K. A., Hearnshaw J. B., Clark M., 1993, ApJ, 413, 349
Nelson B. E., Ford E. B., Payne M. J., 2014a, ApJS, 210, 11
Nelson B. E., Ford E. B., Wright J. T., Fischer D. A., von Braun K., Howard A. W., Payne M. J., Dindar S., 2014b, MNRAS, 441, 442
Nelson B. E., Robertson P., Payne M. J., Pritchard S. M., Deck K. M., Ford E. B., Wright J. T., Isaacson H. T., 2016, MNRAS, 455, 2484
Pérez Martínez M. I., Schröder K.-P., Cuntz M., 2011, MNRAS, 414, 418
Pfahl E., Muterspaugh M., 2006, ApJ, 652, 1694
Portegies Zwart S. F., McMillan S. W. L., 2005, ApJ, 633, L141
Povich M. S., Giampapa M. S., Valenti J. A., Tilleman T., Barden S., Deming D., Livingston W. C., Pilachowski C. 2001, AJ 121, 1136
Quarles B., Cuntz M., Musielak Z. E., 2012, MNRAS, 421, 2930
Queloz D. et al., 2000, A&A, 354, 99
Queloz D. et al., 2001, A&A, 379, 279
Rafikov R. R., 2013, ApJ, 765, L8
Rafikov R. R., Silsbee K., 2015, ApJ, 798, 71
Rajpaul V., Aigrain S., Roberts S., 2016, MNRAS, 456, 6
Ramm D. J., 2004, PhD thesis, Univ. Canterbury
Ramm D. J., 2008, MNRAS, 387, 220
Ramm D. J., 2015, MNRAS, 449, 4428
Ramm D. J., Pourbaix D., Hearnshaw J. B., Komonjinda S., 2009, MNRAS, 394, 1695
Santos N. C., Mayor M., Naef D., Pepe F., Queloz D., Udry S., Blecha A., 2000, A&A, 361, 265
Skuljan J., 2004, in Kurtz D. W., Pollard K., eds, ASP Conf. Ser. Vol. 310, IAU Colloq. 193: Variable Stars in the Local Group. Astron. Soc. Pac., San Francisco, p. 575
Skuljan J., Ramm D. J., Hearnshaw J. B., 2004, MNRAS, 352, 975
Slee O. B., Stewart R. T., Bunton J. D., Beasley A. J., Carter B. D., Nelson G. J., 1989, MNRAS, 239, 913
Sterne T. E., 1941, Proc. Natl. Acad. Sci., 27, 175
Thébault P., 2011, Celest. Mech. Dyn. Astron., 111, 29
Trilling D. E. et al., 2007, ApJ, 658, 1264
Tutukov A. V., Fedorova A. V., 2012, Astron. Rep., 56, 305
Walker G. A. H., 2012, New Astron. Rev., 56, 9
Walker G. A. H., Yang S., Campbell B., Irwin A. W., 1989, ApJ, 343, L21
Walker G. A. H., Bohlender D. A., Walker A. R., Irwin A. W., Yang S. L. S., Larson A., 1992, ApJ, 396, L91
Wang J., Xie J.-W., Barclay T., Fischer D. A., 2014, ApJ, 783, 4
Warner B., 1969, MNRAS, 144, 333
Wittenmyer R. A., Endl M., Wang L., Johnson J. A., Tinney C. G., O'Toole S. J., 2011, ApJ, 743, 184
Wright J. T., Eastman J. D., 2014, PASP, 126, 838
Wright J. T. et al., 2013, ApJ, 770, 119
Zhou J.-L., Xie J.-W., Liu H.-G., Zhang H., Sun Y.-S., 2012, Res. Astron. Astrophys., 12, 1081
Zucker S., Mazeh T., Santos N. C., Udry S., Mayor M., 2004, A&A, 426, 695

SUPPORTING INFORMATION

Additional Supporting Information may be found in the online version of this article:

Table 3. An abbreviated list of the 1180 AUSTRAL-processed I_2 spectra acquired during 2009–2013 using the 4k × 4k CCD including barycentric-corrected Julian date, corrected relative velocity V_{I_2}, internal error σ_i and barycentric correction, and the S/N in order $n = 110$.
Table 4. An abbreviated list of the relative velocity data of 32 4k × 4k detector observations acquired 2006–2013 using CCF fitting. Columns as for Table 3.
Table 5. An abbreviated list of the 225 spectra acquired during 2001–2007 using the 1k × 1k CCD. Columns as for Table 3.

(http://www.mnras.oxfordjournals.org/lookup/suppl/doi:10.1093/mnras/stw1106/-/DC1).

Please note: Oxford University Press is not responsible for the content or functionality of any supporting materials supplied by the authors. Any queries (other than missing material) should be directed to the corresponding author for the article.

This paper has been typeset from a TEX/LATEX file prepared by the author.